Crystallization behavior of as-deposited, melt quenched, and primed amorphous states of $Ge_2Sb_{2.3}Te_5$ films

Cite as: Journal of Applied Physics **88**, 3926 (2000); https://doi.org/10.1063/1.1289811
Submitted: 04 January 2000 . Accepted: 28 June 2000 . Published Online: 19 September 2000

Pramod K. Khulbe, Ewan M. Wright, and Masud Mansuripur

Crystallization behavior of as-deposited, melt quenched, and primed amorphous states of $Ge_2Sb_{2.3}Te_5$ films

Pramod K. Khulbe,[a] Ewan M. Wright, and Masud Mansuripur
Optical Science Center, University of Arizona, Tucson, Arizona 85721

(Received 4 January 2000; accepted for publication 28 June 2000)

We compare the crystallization behavior of thin films of $Ge_2Sb_{2.3}Te_5$ in various amorphous states, namely, as-deposited, melt-quenched, and primed. These films are embedded in a quadrilayer stack similar in structure to the commercially available phase-change optical disks. This study shows that the melt-quenched amorphous film has a shorter crystallization onset time and a higher crystallization rate in comparison to the as-deposited amorphous film. We also observed that variable priming leads to crystallization behavior falling between that of the as-deposited and melt-quenched states. A qualitative model of the modification in crystallization behavior due to priming is given based on the notion that priming produces crystalline embryos which hastens crystallization process. © *2000 American Institute of Physics*. [S0021-8979(00)09219-7]

I. INTRODUCTION

In phase change (PC) optical data storage, information is recorded as submicron sized amorphous marks (bits) on a moving polycrystalline chalcogenide film using a focused, high power laser pulse through a high numerical aperture (NA) lens. The focused laser pulse raises the local temperature of the film above its melting point and the subsequent rapid cooling leaves an amorphous mark on the film. By scanning this trail of amorphous marks by the same laser operating in cw mode at a lower power, data bits can be read through amplitude (or phase) modulation of the reflected light. The intensity (and phase) modulation of the reflected light arises from the large difference in optical constants (n, k) between the polycrystalline and amorphous states of the chalcogenide film. These amorphous marks can also be erased (i.e., recrystallized) by locally annealing them above the glass transition temperature of the chalcogenide material under the same focused laser beam at a moderate power level. In actual devices the PC film is sandwiched between dielectric layers and incorporated into an optimized quadrilayer stack (as in Fig. 1) to control the heating and cooling rates during recording and erasure. The quadrilayer stack is also optimized for a desirable amplitude (or phase) modulation of the reflected light during readout. By modulating the laser power at erase (i.e., moderate) and write (i.e., high) power levels, direct overwriting is achieved. Ohta *et al.*[1,2] and Akahira *et al.*[3] have excellently summarized the basic concepts of optical data storage.

In general, melting is a faster process than crystallization. Thus, for direct overwriting by one laser spot, the crystallization speed of melt-quenched amorphous marks becomes the limiting speed. Crystallization studies of as-deposited amorphous films frequently give crystallization times that are much too long for any high-speed data storage application.[4] Fortunately, however, these crystallization times are not relevant to optical recording because of the substantial differences between the as-deposited and melt-quenched amorphous states.[1,4] The difference between crystalline and amorphous phases of the storage material is well known, and is amply described in terms of the structural and optical parameters of the two states.[1–3, 5] However, the difference between the as-deposited and melt-quenched amorphous states is not so straightforward.[4] It is not known why the crystallization onset time in the as-deposited amorphous state could exceed that of the melt-quenched state by as much as an order of magnitude. Furthermore, the as-deposited state could be transformed via variable optical irradiation into a ''primed'' amorphous state, which displays crystallization behavior approaching that of the melt-quenched state. In this article, we present a systematic study of the crystallization behavior of GST media in a static tester[6] starting from various initial amorphous states to elucidate a qualitative physical mechanism responsible for above observations.

II. EXPERIMENTAL CONDITIONS

Figure 1 shows a typical quadrilayer PC optical disk stack deposited on a 1.2 mm thick polycarbonate substrate. The stack consists of a 77-nm-thick lower dielectric layer ($ZnS–SiO_2$), a 25-nm-thick $Ge_2Sb_{2.3}Te_5$ layer (hereafter referred to as GST), a 25-nm-thick upper dielectric layer ($ZnS–SiO_2$), and a 100-nm-thick aluminum–chromium (Al–Cr) alloy reflector layer. The values of optical and thermal constants of these layers are listed in Table I.

The crystallization experiments were conducted on a two-laser static tester, which is built around a commercial polarization microscope (Olympus, U-PMTVC). As the name suggests, it is equipped with two semiconductor diode lasers operating at $\lambda_1 = 680$ nm (laser 1) and $\lambda_2 = 643$ nm (laser 2). Both lasers are focused simultaneously and coincidentally on the PC layer of the sample through a microscope objective from the substrate side (see Fig. 1). The light reflected from the sample is collected by the same objective lens and sent through a glass prism, which separates two

[a]Electronic mail: pkkhulbe@u.arizona.edu

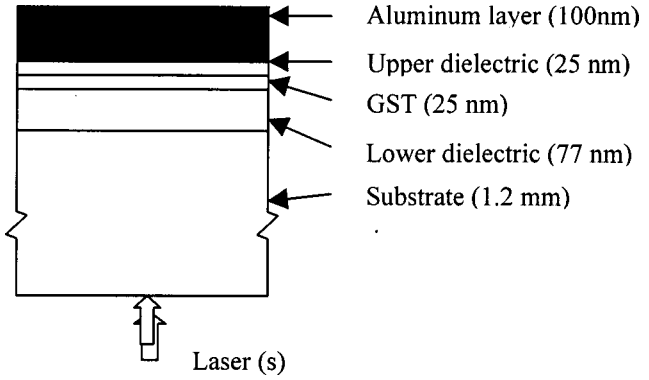

FIG. 1. Structure of a quadrilayer phase-change optical disk used in the present study. The optical and thermal constants of the various layers are listed in Table I. Two laser beams are focused on the GST layer through the substrate by a microscope objective, corrected for the 1.2 mm thickness of the substrate.

laser beams and directs them towards separate photodetectors. The detector outputs are fed to a digital oscilloscope and a computer for further processing. We use laser 1 in a variable power/duration pulsed mode to write crystalline marks on as-deposited, melt quenched, and primed amorphous GST films. Laser 2 is operated in a low power cw mode ($P_2 \sim 0.19$ mW) for real-time monitoring of the local reflectivity variation (i.e., starting from prior to turning on of laser 1 pulse until long after the laser pulse is turned off) during crystalline mark formation. The detector signal of laser 1 can also be utilized for reflectivity measurement, however it would provide reflectivity variation only for the duration of the pulse. Since this information is already included in the detected signal of laser 2, we can disregard the detector output associated with laser 1 for the present set of experiments. The focused spot diameters of both lasers at full width at half maximum (FWHM) intensity are measured to be ~ 0.6 μm when a 0.8 NA microscope objective is used. A white light source illuminates the field of view of the objective lens, where the sample (Fig. 1) is placed on an x-y translation stage. The field of view of the microscope objective is read by a CCD camera and displayed on a CCTV for a visual inspection of crystalline marks on amorphous GST film (or vice versa). Details of the construction and functioning of the tester are given elsewhere.[6]

The reflectance of the samples is calibrated against a polished silicon surface, having a nominal reflectivity of 33% at 643 nm. The silicon sample has a large thermal conductivity and, therefore, its reflectance is not expected to change significantly as it absorbs energy from the focused laser beam.

TABLE I. Optical and thermal constants of various materials of the quadrilayer disk used for evaluating the temperature profile.[a]

	Refractive index $n+ik$ (at $\lambda = 643$ nm)	Specific heat C (J/cm^3/°C)	Thermal conductivity K (J/cm/s/°C)
Polycarbonate (substrate)	1.58	1.70	0.0022
Aluminum alloy	$1.9+i6.2$	2.45	0.400
$Ge_2Sb_{2.3}Te_5$ (amorphous)	$4.3+i1.7$	1.3	0.002
$Ge_2Sb_{2.3}Te_5$ (crystalline)	$4.8+i4.2$	1.3	0.005
$ZnS-SiO_2$ (dielectric)	2.09	2.0	0.006

[a]The laser focus spot size (at FWHM) for 0.8, 0.6, 0.4 NA microscope objectives is 0.60, 0.82, and 1.51 μm, respectively.

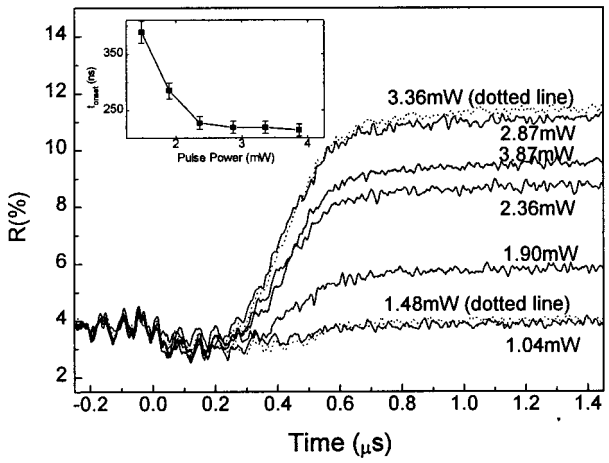

FIG. 2. Reflectivity variations during crystallization of the as-deposited GST film. Different curves correspond to different values of the laser pulse power, as indicated on the right-hand side of each curve. All the pulses have a 0.5 μs pulse width. The highly correlated oscillations below 0.3 μs are associated with the functioning of the static tester and should be disregarded.

III. CRYSTALLIZATION OF AS-DEPOSITED AMORPHOUS SAMPLE

Figure 2 shows the variations in reflectivity (R) during formation of crystalline marks on an as-deposited amorphous GST film upon application of a 0.5-μs-long rectangular pulse (pulse range: 0–0.5 μs on the horizontal axis in Fig. 2). The pulse power in this experiment is varied in discrete steps from 1.04 to 3.87 mW, as indicated on the corresponding curves in Fig. 2. Laser 2, which operates at low power ($P_2 \sim 0.19$ mW) in the cw mode, monitors the changing reflectivity during and after the pulse from laser 1, thus providing information about both the heating and cooling cycles. Both lasers were focused onto the sample with the help of a 0.8 NA microscope objective.

Most of the features of reflectivity curves during the crystalline mark formation on as-deposited amorphous GST are well understood.[4,5,7] Here we will reiterate some of the features, which are relevant to compare the crystallization behavior of various amorphous states. In Fig. 2, for all values of pulse power (P_1), R starts at the amorphous state reflectivity ($R_a \sim 4\%$) and, once the pulse is triggered, drops a little in the beginning, until the temperature exceeds the critical temperature for crystallization at the center of the focused spot. With the onset of crystallization, R begins to rise as the crystalline mark expands outward. The final value of reflectivity in this experiment never reaches to that of a fully crystalline sample ($R_c \sim 18\%$), because the size of the final crystalline mark remains smaller than the probe laser's focused spot size. Additionally, this could be due to the fact that the crystalline mark may still have some amorphous material left within it. It is important to note that the crystallization onset time decreases with the increasing power P_1 of the laser

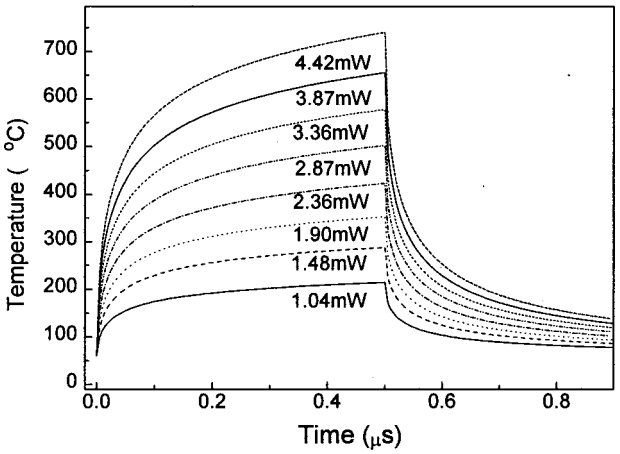

FIG. 3. Simulated temperature profiles at the center of the focused spot on GST film for the quadrilayer disk structure shown in Fig. 1. The pulse powers indicated in the figure are actual pulse powers used for the crystallization of various amorphous states.

pulse, which saturates at ~0.23 μs as shown in the inset of Fig. 2. It indicates the existence of a minimum ''incubation'' time required to trigger the crystallization of the as-deposited amorphous GST. As pointed out earlier, this crystallization onset time is too long for direct overwrite applications in an optical disk. In Fig. 2 we observe an optimum pulse power to achieve the maximum crystallization. This optimum value is 3.36 mW, which gives the maximum value of final reflectivity. If we increase the value of P_1 above 3.36 mW, we see a reduction in the crystallization rate and final reflectivity value. This is because at higher power the temperature at the center of the focus spot could exceed the melting point of the GST.[5] The small initial drop in the reflectivity in the early stages of heating is likely caused by the variation of the optical constants of the sample with the rising temperature. As a test of this conjecture, by terminating the laser pulse before the onset of crystallization and monitoring the subsequent change in reflectivity, we have observed that the initial drop in the reflectivity is reversible,[7] as expected from a thermal effect. After $t=0.5\,\mu$s, when the laser 1 pulse is turned off, we observe that reflectivity continues to increase for a while. There are four possible sources for this behavior to varying extent: (i) further crystallization of GST within the partially crystallized mark, (ii) expansion of crystalline mark at the mark boundary, (iii) return of the optical constants of one or more layers of the quadrilayer stack to their room temperature values, and (iv) recrystallization of the central melt (applicable only for $P_1>3.36$ mW).

Figure 3 shows temperature variation at the center of the laser focus on GST film under pulse powers used in Fig. 2. These temperatures profiles are evaluated by solving heat diffusion equations using a computer program TEMPROFILE.[8–10] These temperature profile calculations are based on an overly simplified assumption that the optical and the thermal constants listed in Table I are temperature independent. The fact remains, however, that the numerical values of the optical and thermal constants of the layers are available at room temperature; even then, at best they are rough estimates. However, it is fortunate that the thermal mass of the sample arises mainly from the dielectric layers, the aluminum layer and the substrate and, therefore temperature profiles shown in Fig. 3 are not very sensitive to the optical and thermal constants of the GST layer. Figure 2 shows that crystallization starts beyond the threshold power $P_1=1.48$ mW. The corresponding temperature profile shown in Fig. 3 indicates that it leads to a peak on-axis temperature $T\sim285\,^\circ$C at $t\sim500$ ns. This temperature should be compared with the critical temperature $T\sim160-170\,^\circ$C for slow crystallization of the same samples over a period of seconds (rather than a few hundred nanoseconds).[11] This discrepancy will be understood automatically, after we introduce a theoretical model for crystallization of GST thin films under pulsed irradiation in Sec. VIII.

Beyond the previously mentioned threshold pulse power, the crystallization rate ($\Delta R/\Delta t$) increases with increasing P_1. The maximum value of $\Delta R/\Delta t$ is obtained at $P_1\sim3.36$ mW. Temperature profile calculations show that this pulse power corresponds to a peak on-axis temperature $T\sim585\,^\circ$C around $t=500$ ns (see Fig. 3). We conclude that the probabilities of crystal nucleation and growth have significant values in the temperature range $T\sim285-585\,^\circ$C in as-deposited amorphous GST films. Above $P_1\sim3.36$ mW, $\Delta R/\Delta t$ declines. For these values of P_1 the temperature of the GST film at the center of the laser spot exceeds the melting temperature ($T_M\sim620\,^\circ$C).[5] Thus, any increase in reflectivity R due to crystallization in the periphery of the laser spot (where the temperatures remain below the melting point) will be offset by the reduction in R caused by the melting at the center.

IV. CRYSTALLIZATION OF THE MELT-QUENCHED AMORPHOUS STATE

To study the crystallization behavior of melt-quenched amorphous state, we conducted the following experiment: A large region of the sample was fully crystallized by a slow x-y scan of a focused cw laser beam operating at ~2.0 mW. The laser beam was focused with the help of a lower NA (0.4 NA) microscope objective, which has a larger focus spot size (~1.51 μm at FWHM) for faster and uniform crystallization. Now we focus a 16.0 mW, 0.5 μs rectangular pulse from laser 1 on the crystallized surface with the help of the same 0.4 NA objective, which raises the temperature in the vicinity of the focused spot above the melting temperature of GST.[5] When this melt cools, an amorphous mark is formed. A repetition of this process creates an array of melt quenched amorphous marks. A visual inspection (after the superposition of known periodic array structure on this array of amorphous marks) indicates that the amorphous marks were ~2.0 μm in diameter. The center of melt quenched amorphous marks was then crystallized at various pulse powers by focusing 0.5 μs long pulses of variable power with the help of a higher NA (0.8 NA) microscope objective. This ensured that during the process of crystalline mark formation at the center of 2.0 μm melt-quenched spot, there was no interference from the crystalline boundary as the size of the recrystallized mark remained smaller than 1.0 μm. The reflectivity

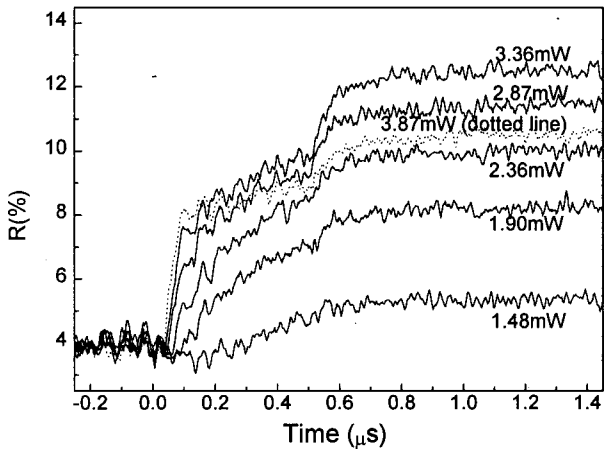

FIG. 4. Reflectivity variations during crystallization of a large melt-quenched region on the GST film. Different curves correspond to different values of the laser pulse power, as indicated on the right-hand side of each curve. All the pulses have a 0.5 μs pulse width. The highly correlated oscillations below 0.3 μs are associated with the functioning of the static tester and should be disregarded.

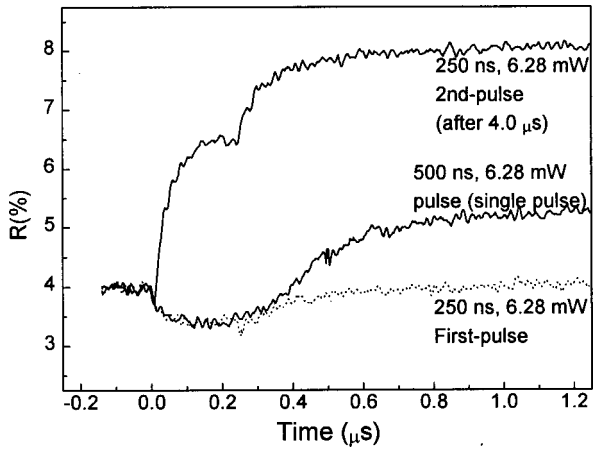

FIG. 5. Reflectivity variations during crystallization of as-deposited GST under three different conditions. In the case of the middle curve a single 6.28 mW, 500 ns pulse was applied to the as-deposited amorphous film. The bottom curve corresponds to a single 6.28 mW, 250 ns pulse, applied to the as-deposited film. The top curve shows the reflectivity variations obtained when a 6.28 mW, 250 ns pulse was applied on a sample ''primed'' by an identical pulse 4 μs earlier.

curves recorded during this experiment are shown in Fig. 4. From the comparison of the reflectivity curves of Figs. 2 and 4 we can make the following observations:

(i) The reflectivity values of as-deposited and melt-quenched states are identical.

(ii) The crystallization onset time is shorter for the melt-quenched amorphous GST as compared with the as-deposited amorphous material.

(iii) Once crystallization is triggered, the initial rate of crystallization $(\Delta R/\Delta t)$ is higher in the melt-quenched material as compared to the as-deposited material.

(iv) The highest value of final reflectivity is obtained by applying a pulse of power $P_1 = 3.36$ mW and duration 0.5 μs for both the as-deposited and melt-quenched states.

(v) Furthermore, the minimum value of P_1 required to trigger crystallization is slightly higher in as-deposited case.

(vi) In melt quenched amorphous GST, the crystallization rate slows down towards the end of laser pulse, whereas in as-deposited case, there is monotonic increase in the reflectivity. In both states, there is a gain in R after laser pulse is turned off at 0.5 μs. Although, in Fig. 4 it is more evident because of an apparent discontinuity in reflectivity curves at $t = 0.5$ μs.

On the basis of observations (i) and (iv), the optical and thermal constants can be assumed to be almost same for the melt-quenched and the as-deposited amorphous GST (see Table I).

V. TWO-PULSE CRYSTALLIZATION AND THE CONCEPT OF PRIMED AMORPHOUS STATE

Figure 5 shows the variation of reflectivity R with time for an as-deposited amorphous GST film under three different conditions: (i) a single pulse of power $P_1 = 6.28$ mW, and duration $(\tau) = 500$ ns, (ii) a single pulse with $P_1 = 6.28$ mW, and $\tau = 250$ ns, and (iii) two identical pulses with $P_1 = 6.28$ mW, and $\tau = 250$ ns with a 4.0 μs gap in between them. In case (iii), Fig. 5 shows the time variation of the second pulse alone. The initial pulse, which is identical to the pulse in case (ii), plays the role of a priming pulse. Also, here P_1 appears higher than in our previous examples because a 0.6 NA microscope objective was employed to focus the laser pulse.

Figure 5 shows that the two-pulse combination (iii) crystallizes the film much more rapidly and completely than the 500 ns long pulse (i), which nonetheless has the same energy. In addition, this is the case even though the initial priming pulse, which is identical to the pulse in case (ii), does not induce crystallization, but modifies the state such a way that now the crystallization is earlier and faster under the influence of second identical pulse. In the literature this modified state of the amorphous film is referred to as the ''primed state.'' [4] Thus, when second pulse is incident on the same spot on the ''primed'' film, the crystallization onset time is reduced and the crystallization speed increases markedly.

VI. MODIFICATION IN CRYSTALLIZATION BEHAVIOR ON CW PRIMING

Reflectivity variations have been measured during crystalline mark formation on GST films primed to various levels. Five priming levels were prepared at various locations on a GST film by x-y scanning of a focused (0.4 NA objective) cw laser beam operating at power levels of 1.28, 1.33, 1.40, 1.46, 1.52, and 1.59 mW, respectively. Next a pulse of power $P_1 = 2.87$ mW and duration 0.5 μs is focused with the help of a 0.8 NA objective onto the various primed regions to study the crystallization behavior. A coincident low power (0.19 mW) cw laser beam measures the reflectivity variation during mark formation. The results are shown in Fig. 6, where we see that the surfaces primed at 1.28 mW show crystallization behavior identical to that of the as-deposited amorphous state in Fig. 2. On priming at higher laser powers, we notice a systematic modification in the crystallization behavior of the GST. In particular, the crystallization onset

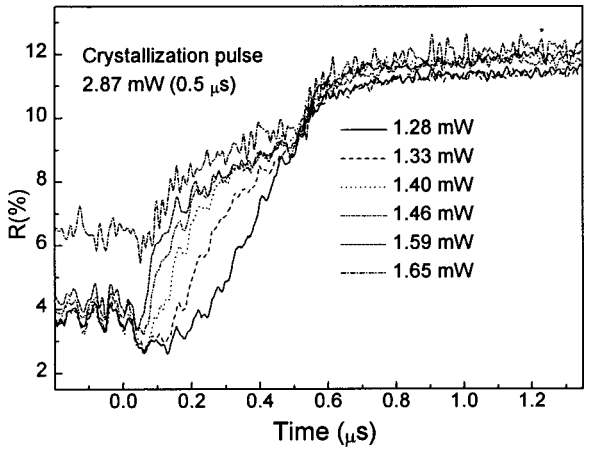

FIG. 6. Reflectivity variations during crystallization of a GST film, which is primed to various levels by x-y scanning at various cw power levels. All curves correspond to reflectivity change during crystallization under 2.87 mW, 0.5 μs long pulse. The highly correlated oscillations below 0.3 μs are associated with the functioning of the static tester and should be disregarded. Relatively higher noise in this figure is due to a lesser number of accumulations made for averaging the reflectivity traces.

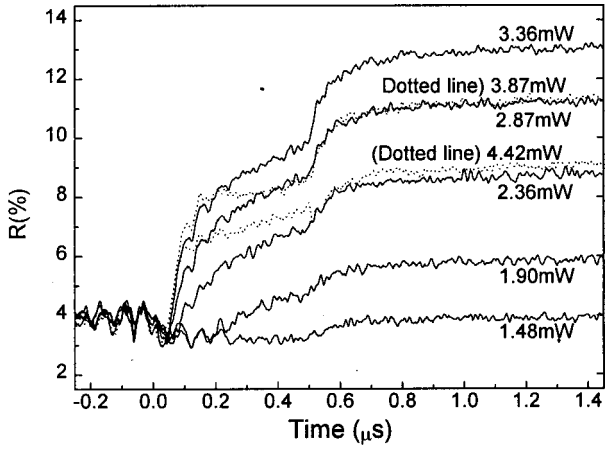

FIG. 7. Reflectivity variations during crystallization of the fully primed GST film. Different curves correspond to different values of the laser pulse power, as indicated on the right-hand side of each curve. All the pulses have a 0.5 μs pulse width. The highly correlated oscillations below 0.3 μs are associated with the functioning of the static tester and should be disregarded.

time decreases and the crystallization rate increases in an earlier part of the laser pulse. It may also be noted that the initial reflectivity (prior to the onset of pulse) remains fixed at ~4% for priming levels below 1.59 mW, which is identical to the reflectivity values of as-deposited and melt quenched amorphous states. This indicates that the optical constants of the primed amorphous state are the same (or nearly the same) as those of as-deposited amorphous and melt-quenched states. On priming the GST film above 1.59 mW cw power, we observe a partial crystallization of the film, whose initial reflectivity is higher than 4%. In Fig. 6 this situation is represented by the reflectivity curve obtained during the crystallization of the area which was scanned by 1.65 mW cw power. We therefore introduce the concept of the fully primed amorphous state, meaning that the priming has progressed as far as it can without inducing some crystallization.

VII. CRYSTALLIZATION BEHAVIOR OF FULLY PRIMED GST FILM

Reflectivity variations have been measured during crystalline mark formation on a fully primed GST film (the primed surface prepared by 1.59 mW cw scanning in the previous experiment) at various pulse powers in the range 1.48–4.42 mW and a 0.5 μs pulse duration. Again both lasers were focused on the GST film with the help of a 0.8 NA microscope objective and the lower power (0.19 mW) cw laser beam measures the reflectivity variation during mark formation. The results are shown in Fig. 7. It is evident that the crystallization behavior in Fig. 7 is almost similar to that of melt quenched amorphous state (Fig. 4) and both crystallization behaviors differ in similar ways from the crystallization behavior of as-deposited GST. The crystallization onset times and the crystallization rates for all three amorphous states of GST are given in Table II.

Apart from the differences listed in Table II, the reflectivity curves of Figs. 4 and 7 differ from those in Fig. 2 in an additional sense. In Fig. 2, when the crystallization is triggered, it proceeds with a constant rate (fairly constant $\Delta R/\Delta t$), unlike in Figs. 4 and 7 (melt quenched and fully primed amorphous states) where the crystallization rate slows down considerably in the later part of the pulse. The initial rapid crystallization leaves a smaller amount of amorphous material available for further crystallization in Figs. 4 and 7, which reduces the crystallization speed in a subsequent part of the pulse. Figure 6 depicts this concept very clearly, in which all crystallization routes end up as the same reflectivity value at the end of the write laser pulse ($t = 0.5\,\mu$s).

VIII. DISCUSSION

The experimental results presented so far need answers to the following questions: (i) why melt-quenched GST shows shorter crystallization onset time and higher crystallization rate as compared to as-deposited GST, and (ii) why priming of as-deposited amorphous films can alter the crystallization behavior towards that of the melt-quenched amorphous state. The goal of this section is to present a qualitative image of how this occurs based on a theory of crystallization of GST media recently developed.[12] This theory is an adaptation of the nucleation theory of liquid droplets from supersaturated vapor due to Frenkel.[13] The basic notion is that as the laser pulse heats the film in its as-deposited state, the amorphous lattice may relax via atomic reordering to produce localized crystalline units of lower free energy, or embryos, throughout the sample. Given this basic crystalline unit, if two embryos are formed in close proximity they may join to form a cluster of two embryos of volume $2V_1$ (V_1 being the volume of single embryo). In general, a cluster of g(g = an integer) embryos can be formed when a single embryo condenses onto a cluster of the size $g-1$. Similarly, evaporative processes can also occur in which a

TABLE II. Comparison of the crystallization behavior.

	Crystallization onset time (t_{onset}) (ns)	Crystallization rate[a] $\Delta R(\%)/\Delta t$ (ns)	Initial reflectivity (%)	Minimum pulse power for crystallization (mW)	Maximum pulse power for crystallization (mW)
As-deposited amorphous GST	~230	~25.25	3.90	1.90	3.36
Fully primed amorphous GST	~30	~72.11	3.90	1.90	3.36
Melt-quenched amorphous GST	~30	~71.39	3.87	1.48	3.36

[a]Crystallization rate is measured immediately after the onset of crystallization.

cluster of size g loses an embryo. The dynamics of crystallization is therefore dictated by the condensation and evaporation of crystalline clusters.[12] We do not need the full dynamics here, but the key idea is that whether a cluster grows in size or shrinks is dictated by the interplay between the increase in free energy due to the surface area of the cluster which is proportional to $g^{2/3}$, and the decrease in the free energy due to the volume of the cluster which is proportional to g.

$$\Delta F_g = Ag^{2/3} - kT\ln(S)g. \tag{1}$$

Here A is a constant proportional to the free-energy per unit area, k is Boltzmann's constant, and S is the supersaturation whose relation to this problem will be elucidated below. For $S>1$, with $S=1$ being the saturated state, the free energy displays a single maximum for a critical cluster size g^* given by

$$g^* = \left(\frac{2A}{3kT\ln(S)}\right)^3, \tag{2}$$

and clusters of size $g>g^*$ tend to grow, and those with $g<g^*$ tend to shrink. In general, the larger g^* is the longer onset time for crystallization from the initial amorphous state: this makes intuitive physical sense since it takes time for clusters to grow to a given size via the processes of condensation and evaporation.[14] In addition, the rate of crystallization I should follow the basic relation[15]

$$I \propto \exp[-\Delta F^*/kT] = \exp[-(A/3kT)(g^*)^{2/3}], \tag{3}$$

at least qualitatively, so we see that the larger the critical cluster size g^* the slower the crystallization rate. Physically, as g^* decreases the free-energy barrier ΔF^* to crystallization also decreases.

We now relate the parameters of the prior discussion to the problem of crystallization of GST media. The key parameter is the supersaturation S, which we previously identified[12] as proportional to the density N_1 of crystalline embryos

$$S = n = \frac{N_1}{N_{1,\text{sat}}}, \tag{4}$$

with $N_{l,\text{sat}}$ the density of embryos at saturation $S=1$. Furthermore, we assumed that the normalized embryo density n, and hence S, should obey a rate equation of the form

$$\frac{\partial S}{\partial t} \propto e^{-(T-T_p)^2/\Delta T^2}, \tag{5}$$

with T_p the temperature of peak embryo generation, and ΔT the temperature range over which embryo generation occurs. Physically, embryo generation via lattice relaxation starts above the glass temperature T_G, whereas for temperatures higher than the melting temperature T_M, the lattice is too hot to allow the embryo formation. Thus, $T_G<T_P<T_M$, with $T_G \sim 160\,^\circ\text{C}$, $T_p \sim 430\,^\circ\text{C}$, and $T_M \sim 620\,^\circ\text{C}$ for our GST medium.[16] The temperature profile simulations carried out for our previously described variable priming experiment (x-y scanning of GST film for cw powers in the range of 1.28–1.59 mW) indicate that the film is exposed to peak temperatures in the vicinity of T_G during the priming process. These temperature simulations are shown in Fig. 8 and use the same approximations, which were used to simulate the temperature profiles shown in Fig. 3.

We now have the ingredients needed to place our experimental results in a theoretical framework. Our basic notion is that the initial as-deposited state is very close to the saturated state $S(t=0)=1$, which according to Eq. (2) has an infinite critical cluster size, and will therefore never crystallize spontaneously. If laser radiation is now applied and the film heats up above the glass temperature, then according to Eq. (5) the density of embryos, and hence the supersaturation $S(t>0)>1$, will be increased with a concomitant reduction of the critical cluster size according to Eq. (2). This is the basic physical mechanism of priming, which involves the creation of crystalline embryos throughout the film without the creation of critical size clusters $g>g^*$, and the key is that these embryos survive in the film even after the irradiation is turned off.

We turn our attention to Fig. 5 where a 6.28 mW, 500 ns pulse begins to creat enough critical size crystalline clusters to start raising the reflectivity from $t \sim 250$ ns onward. This happens after the beginning portion of the pulse has created

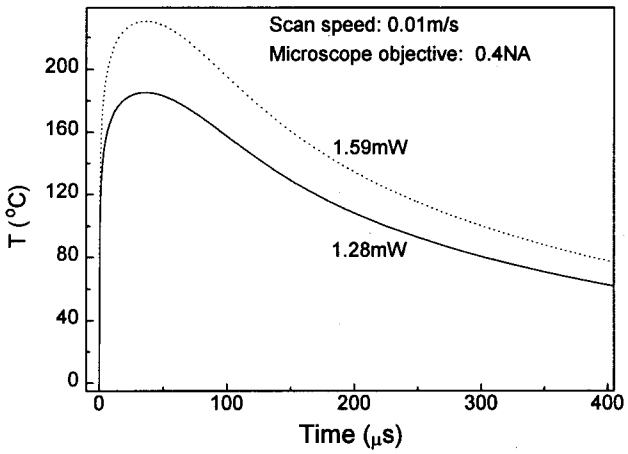

FIG. 8. Simulated temperature profiles at any point on the surface of GST film in the disk structure shown in Fig. 1 while priming the GST surface by *x*-*y* scanning of a cw laser beam. The scanning speed was 0.01 m/s, and laser beam was focused with 0.4 NA microscope objective. 1.28 mW laser power starts priming GST surface and laser power above 1.59 mW which is the maximum priming power needed for the priming without crystallizing the GST film.

enough embryos according to Eq. (5). In the case of 6.28 mW, 250 ns single pulse we terminate the laser pulse before the critical clusters start forming, so that the reflectivity remains unchanged. However, this pulse creates enough embryos, not only during the pulse when the film is heated, but also after the pulse when the sample returns to room temperature. This temperature cycling process produces a large number of embryos according to Eq. (5), which increases the supersaturation and reduces the critical cluster size, a condition more favorable for crystallization. Therefore, when the second pulse is irradiated after 4.0 μs, we observe a significantly shorter crystallization onset time and higher crystallization rate with respect to the as-deposited GST. Similar mechanism works when we prime the GST film to a varying degree, as is the case in Fig. 6. Figure 8 shows temperature variation with time at any point on GST film when we scan it under 1.28 and 1.59 mW cw laser power beam at 0.01 m/s speed. This power level range exposes the film to a temperature range $\sim$180–235 °C, which is just above the glass transition temperature of GST. Clearly as the scanning power is increased sequentially from 1.28 to 1.59 mW, GST film spends more and more time above the glass transition temperature and also simultaneously encounters higher embryo generation rate according to Eq. (5). The embryos once produced survive even after removing the laser beam. Thus, a sequential increase in supersaturation and a sequential reduction in critical cluster size occur, a condition more and more favorable for crystallization. This explains the systematic modification in the crystallization behavior of the GST film depicted in Fig. 6. On increasing the priming power above 1.59 mW, we let this process go beyond, when the critical size crystalline clusters actually start forming during scanning itself. Similarly, during the formation of melt quenched amorphous mark when the molten pool of GST cools through $T_M \rightarrow T_p \rightarrow T_G$, it is expected to gain a significant embryo content [see Eq. (5)]. However, it is quite coincidental that the gain in embryos in melt quenched mark formation is comparable to the gain in embryos in fully primed case. That is why we see a close similarity in crystallization behaviors depicted by Figs. 4 and 7. Strictly speaking, the crystallization behavior of the melt quenched state is slightly better than the crystallization behavior of fully primed GST. This is evidenced by a slightly lower minimum threshold power required for the crystallization of melt-quenched amorphous state.

The above model therefore provides a physical framework in which to view the experimental results: the as-deposited state is identified as the saturated state $S=1$, and priming produces crystalline embryos in the film which act as a seed for crystallization by subsequent pulses. Since priming provides a seed, it is physically reasonable that increasing the priming should reduce the onset time for crystallization and also increase the rate of crystallization. However, eventually the priming itself will result in some crystallization, which led to the notion of the fully primed state, that is, the state with maximum priming which still retains the optical properties of the as-deposited state. Here we found that the melt quenched and fully primed states have very close crystallization behaviors, suggesting that they are physically equivalent in a sense that both have a significant number of embryos embedded in the film. This is not unreasonable since the melt-quenched amorphous state is expected to gain a significant embryo content as a result of the rapid cooling of the melt through the temperature range $T_M \rightarrow T_p \rightarrow T_G$ of maximum embryo generation [see Eq. (5)].

IX. CONCLUSIONS

By monitoring the crystallization behavior of various amorphous GST samples under a focused laser beam we found that the crystallization onset time in melt-quenched amorphous GST sample is significantly shorter than that of as-deposited GST film. We also observed that the crystallization rate of the melt-quenched film is higher than that of the as-deposited film under identical crystallization conditions. Furthermore, the crystallization rates and crystallization onset times are approximately the same for melt quenched and fully primed amorphous states.

We have given a physical image to understand these results occur during priming and melt quenching embryos which get seeded into the media. The crystallization process involves formation of embryos followed by the condensation and evaporation of embryos to form crystalline clusters. Therefore, crystallization in melt quenched and primed GST begins with an advantage because of the embryo seeding, leading to a reduced crystallization onset time and higher crystallization rate. Variable levels of priming can be achieved by controlling the concentration of the embryos generated in the film by exposing it to different temperatures just above glass transition temperature.

ACKNOWLEDGMENTS

The authors are grateful to T. Ohta and T. Nagata of the Matshushita Electric Industries Corp. of Japan for providing the phase-change samples used in this study. This work has

been sponsored in part by the Optical Data Storage Center at the University of Arizona and by Department of Commerce through the NSIC/MORE Program (Cooperative Agreement No. 70NANB7H3054).

[1] T. Ohta, N. Akahira, S. Ohara, and I. Satoh, Optoelectron., Devices Technol. **10**, 361 (1995).
[2] T. Ohta, K. Nagata, I. Satoh, and R. Imanaka, IEEE Trans. Magn. **34**, 426 (1998).
[3] N. Akahira, N. Miyagawa, K. Nishiuchi, Y. Sakaue, and E. Ohno, Proc. SPIE **2514**, 294 (1995).
[4] J. H. Coombs, A. P. J. M. Jongenelis, W. van Es-Spiekman, and B. A. J. Jacobs, J. Appl. Phys. **78**, 4906 (1995).
[5] N. Yamada, E. Ohno, K. Nishiuchi, and N. Akahihara, J. Appl. Phys. **69**, 2849 (1991).
[6] M. Mansuripur, J. K. Erwin, W. Bletscher, P. K. Khulbe, K. Sadeghi, X. Xun, A. Gupta, and S. B. Mendes, Appl. Opt. **38**, 7095 (1999).
[7] P. K. Khulbe, X. Xun, and M. Mansuripur, Appl. Opt. **39**, 2359 (2000).
[8] The simulations were performed with TEMPROFILE™, a product of MM Research, Inc., Tucson, AZ.
[9] M. Mansuripur, G. A. N. Connell, and J. W. Goodman, Appl. Opt. **21**, 1106 (1982).
[10] M. Mansuripur and G. A. N. Connell, Appl. Opt. **22**, 666 (1983).
[11] C. Peng and M. M. Mansuripur, Appl. Opt. **39**, 2347 (2000).
[12] E. M. Wright, P. K. Khulbe, and M. Mansuripur, Appl. Opt. (submitted).
[13] J. Frenkel, *Kinetic Theory of Liquids* (Dover, New York, 1955), Chap. VII.
[14] F. J. M. Farley, Proc. R. Soc. London, Ser. A **212**, 530 (1952).
[15] J. E. McDonald, Am. J. Phys. **30**, 870 (1962); **31**, 31 (1963).
[16] C. Peng, L. Cheng, and M. Mansuripur, J. Appl. Phys. **82**, 4183 (1997).